Depth-Sensitive Raman Spectroscopy of Intact Formalin-Fixed and Paraffin-Embedded Tissue Blocks for Objective Diagnosis of Cancer- An Exploratory Study

Khan Mohd. Khan[1], Hemant Krishna[1], Chandrahas V. Kulkarni[2] and Shovan K. Majumder[1,*]

[1]*Homi Bhabha National Institute, Raja Ramanna Centre for Advanced Technology, Indore 452 013, India*

[2]*Mahatma Gandhi Memorial Medical College, Indore 452001, India*

Abstract: Histopathology, the current "gold standard", is prone to human errors as it depends on expert interpretation of the microscopically derived cellular and sub-cellular information for tissue diagnosis. Further, this light microscope based approach requires preparation of appropriately stained specimens of micro-thin tissue sections from the formalin-fixed and paraffin-embedded (FFPE) blocks of tissue samples. We report a method that provides quantitative feedback about tissue diagnosis by measuring depth-sensitive Raman spectra from the intact FFPE tissue blocks without requiring preparation of any thin tissue sections or any other processing. The FFPE blocks of pathologically certified cancerous and normal breast tissues were used for validating the approach. The measured depth-sensitive Raman spectra were mathematically de-paraffinized for retrieving the characteristic tissue Raman signatures using scaled-subtraction. A multivariate analysis of the scaled-subtracted, depth-sensitive Raman spectra employing a probability-based diagnostic algorithm developed using the framework of sparse multinomial logistic regression (SMLR) provided a sensitivity and specificity of up to 100% towards cancer based on leave-one-block-out cross validation. The results of this exploratory study suggest that depth-sensitive Raman spectroscopy along with a multivariate statistical algorithm can provide a valuable alternate diagnostic modality in clinical pathology setting for discriminating cancerous from normal FFPE tissue blocks.

Keywords: Formalin-fixed and paraffin-embedded (FFPE) tissue blocks, Depth-sensitive Raman spectroscopy, Scale-subtraction.

1. INTRODUCTION

Excisional biopsy followed by histopathology is the current gold standard for definitive diagnosis of cancer. The method makes use of a light microscope to analyse high-resolution image information of cellular and sub-cellular structures of properly pre-processed and appropriately stained specimens of thin tissue sections obtained by microtomy from the formalin-fixed and paraffin-embedded (FFPE) tissue blocks [1-2]. Despite its huge success, a major drawback of this traditional approach is that the diagnosis depends on the expert interpretation of the microscopically derived histopathological information that suffers from both human as well as sampling errors [3]. This is particularly a concern in the context of diagnosing tumors that are atypical or lack morphological features useful for differential diagnosis. An alternate technique that may help overcome these limitations and has recently shown considerable promise for cancer diagnosis using FFPE tissue sections is the technique of Raman spectroscopy [4-9]. Its attractiveness comes from its chemical specificity which enables it to discern the pathological state of the paraffin embedded tissue sections in a non-destructive manner.

In the several studies reported thus far [4-9], micro-Raman spectra were recorded from micro-thin tissue sections obtained by microtomy from the FFPE tissue blocks for differential diagnosis of cancer. However, a common major hurdle faced in all these studies was the orders of magnitude stronger paraffin Raman signal which swamped the rather weak tissue Raman signal. Therefore, faithful retrieval of the tissue Raman signatures from the measured Raman spectra of the FFPE tissue sections posed an important immediate task. Over the years, various efforts of varying rigor were made by the researchers to eliminate the influence of paraffin Raman signatures [4-11]. One approach, followed earlier, was to use chemical de-paraffinization prior to measuring Raman spectra from these de-paraffinized tissue sections [4]. Several chemical methods were investigated for de-paraffinizing the embedded tissue sections. The results of these investigations showed that none of the de-paraffinizing procedures employed was able to completely remove paraffin whose Raman cross-section is known to be much larger compared to that of biological tissue and consequently, the de-paraffinized tissue Raman spectra were found to be severely contaminated with Raman signatures of the residual paraffin thereby masking the differences between spectral profiles of de-paraffinized normal and abnormal tissues. The other approach followed recently

*Address correspondence to this author at the Optical Spectroscopy and Diagnostic Lab, R & D Block-A1, Raja Ramanna Centre for Advanced Technology, Indore 452 013, India; Tel: 91-731-2488437; Fax: 91-731-2488425; E-mail: shkm@rrcat.gov.in, shovan.k.majumder@gmail.com

ISSN: 1927-7210 / E-ISSN: 1927-7229/16

[9-11] was to employ mathematical de-paraffinization to retrieve the tissue specific Raman signatures from the statistical analysis of the set of measured micro-Raman spectra of the micro-thin tissue sections. While the results of these studies demonstrated the applicability of micro-Raman spectroscopy along with mathematical de-paraffinization as a useful way of discerning the diagnostic information from the micro-thin tissue sections prepared from the FFPE tissue blocks, the major disadvantage was that these involved a mathematical model which required a large number of micro-Raman spectra of the micro-thin tissue sections at its input for generating the model source spectra (of paraffin). Another significant disadvantage of the approach was that it was not fully non-destructive since it required the intact FFPE tissue blocks microtomed into thin sections (~5-10 μm) prior to the measurement of micro-Raman spectra from these sections.

We report here a technique which is capable of providing quantitative diagnostic feedback about the tissue under interrogation by measuring depth-sensitive Raman spectra from the intact FFPE tissue blocks without requiring preparation of any micro-thin tissue sections or any other processing. It uses scaled subtraction, a non-statistical method requiring only two spectra, for the mathematical de-paraffinization of the measured depth-sensitive Raman spectra. The approach was validated by measuring depth-sensitive Raman spectra from the FFPE blocks of pathologically certified cancerous and normal breast tissues. The measured spectra were de-paraffinized by subjecting them to scaled-subtraction. A multivariate analysis of the scaled-subtracted, depth-sensitive Raman spectra using a probability-based diagnostic algorithm developed based on the theory of sparse multinomial logistic regression (SMLR) provided a sensitivity and specificity of up to 100% towards cancer based on leave-one-block-out cross validation. The results suggest that depth-sensitive Raman spectroscopy along with a multivariate statistical algorithm has promising potential to be used as an alternate diagnostic modality in clinical pathology setting for discriminating cancerous from normal FFPE tissue blocks.

2. MATERIALS & METHODS

2.1. Instrumentation

A schematic of the experimental setup for the depth-sensitive Raman spectroscopic measurements is shown in Figure **1**. The system utilizes a 785 nm single-mode diode laser (DL785-100-SO, CrystaLaser) as the illumination source. The laser beam is first collimated with an achromat doublet lens (AC254-035-B-ML, Thorlabs Inc.). The collimated laser beam is spectrally purified using a laser clean-up filter (HQ782/20X, Chroma Tech. Corp.). A dichroic filter (λ_{trans}-800 nm, LPD01-785RU-25, Semrock Inc.) kept at an angle of 45° with respect to the lens axis is used to steer the collimated beam towards a mirror kept at an angle of 45° with respect to the beam axis. The mirror reflects the collimated beam towards the sample arm where it is focused through a microscope objective lens (NA = 0.65, 40OM65, Comar Optics) onto the surface of the sample kept on a micrometer-controlled X-Y-Z stage. The Raman signal backscattered from the sample is passed through the same objective lens, reflected by the same mirror and then transmitted by the same dichroic filter (that transmits light above 800 nm) to get steered towards the Raman detection end by passing it through a notch filter (Narrow Notch-6, Tydex J. S. Co.) that filters the elastically scattered light (Rayleigh light). The filtered Raman beam is then focused by another achromat doublet lens (AC254-035-B-ML, Thorlabs Inc.) onto a 100 μm core diameter optical fiber (QMMJ-55-IRVIS-100/140-0.3) coupled to the entrance port of an imaging spectrograph (Acton SP2300, Princeton Instruments) equipped with a thermoelectrically cooled, back-illuminated, deep-depletion CCD camera (Pixis 100, Princeton Instruments). The spectrograph and the CCD camera are controlled with a computer for depth-sensitive Raman spectral measurement.

2.2. Samples

The study involved pathologically characterized FFPE blocks of breast tissue samples obtained from the archival files of the Pathology Department of Mahatma Gandhi Memorial Medical College, Indore. The diagnostic report provided by the histopathologist was taken as the “Gold Standard”. The FFPE tissue blocks consisted of seven invasive ductal carcinoma and seven normal breast tissue samples from a total of 14 different individuals. The paraffin blocks were of 25 mm (L) x 22 mm (B) x 18 mm (H) in dimension. The embedded tissue samples were generally irregular in shape and their surface dimensions ranged from 5 mm x 6 mm to 20 mm x 18 mm.

2.3. Parameters of the Depth-Sensitive System

Our primary goal was to measure depth-sensitive Raman spectra from the FFPE tissue blocks using the

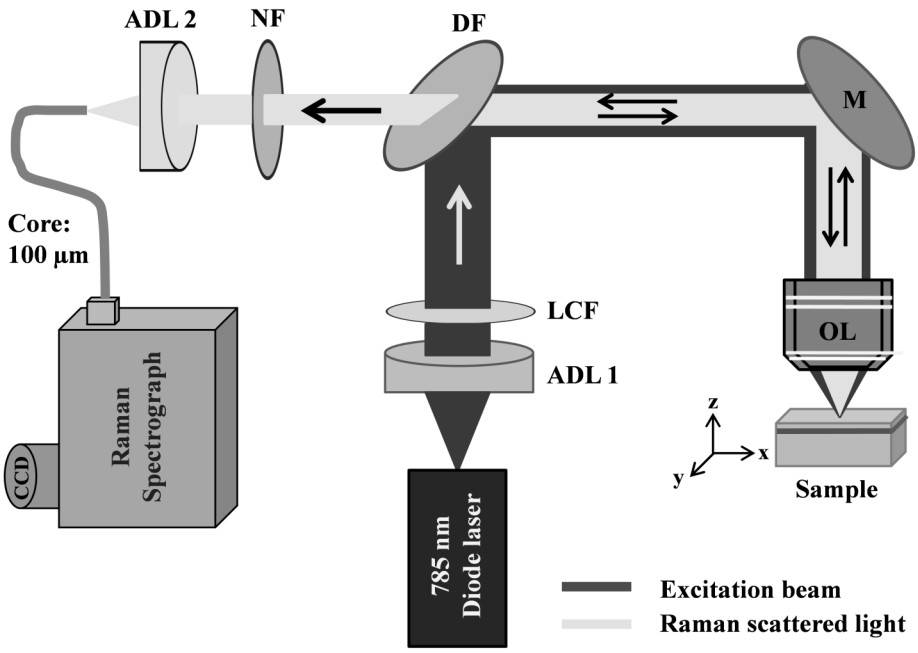

Figure 1: Experimental setup for the depth-sensitive Raman spectral measurements from the FFPE tissue blocks. The abbreviations and their corresponding expanded forms are as follows: ADL-achromat doublet lens, LCF-laser clean-up filter, DF-dichroic filter, M-mirror, OL-objective lens, NF-notch filter.

Raman system developed for that purpose. Thus an important task was to determine the depth resolution of the system. This was done by following the method detailed in our earlier paper [12]. In brief, the Raman spectra were measured by axially moving a 10 µm thick sheet of polymethylacrylate (PMMA) across the focus of the Raman excitation beam and then fitting a Gaussian to the plot of the intensities of the characteristic Raman peak of PMMA (at 1450 cm^{-1}) versus the axial distance. The full width at half maximum (FWHM) of the fitted Gaussian, measured to be ~50 µm, was taken as a practical estimate of depth resolution of the system.

The spot size at the focal plane was estimated by following the edge response method described elsewhere [13]. In this method, the focus of the Raman excitation beam was laterally scanned over a clean edge of a PMMA layer of thickness 10 µm and the fall in the intensity of the 1450 cm^{-1} Raman peak was noted. An error function was fitted to the measured Raman intensities. The lateral movement of sample stage corresponding to the point where the intensity dropped to $1/e^2$ was taken as a measure of the spot size which was found to be ~7 µm.

The signal-to-noise ratio (SNR) of the system, defined as the ratio of the maximum intensity of the signal to the baseline noise, was calculated as SNR = (signal maximum-signal minimum) / (baseline standard deviation in non-Raman region) and found out to be ~600 for the 1382 cm^{-1} naphthalene Raman peak for an integration time of 1 s.

2.4. Experimental Measurements and Data Processing

For the measurement of Raman spectra from the various depths of a FFPE tissue block, the focal plane of the Raman excitation beam was shifted axially (in z-direction) by moving the tissue block kept on the micrometer-controlled stage along the axial direction. For generating good quality Raman spectra, the integration time used was 10 s. The optical power onto the target sample was measured to be ~50 mW for the illumination beam.

For each measured Raman spectrum, the wavenumber axis was calibrated with the illumination laser line, acetaminophen and naphthalene standards, and the spectrum was truncated over the region 800-1800 cm^{-1} to avoid the interference of the Raman peaks due to the silica as well as the noise present at the far end of the spectral region. A blank spectrum (considered as the dark signal) acquired in absence of any light source prior to spectral measurements in a sample was subtracted from the corresponding spectra and the subtracted spectra were then corrected for the spectral response of the system by using an NIST traceable calibration lamp (LS-1, Ocean Optics) [14].

The corrected spectra were then fed to the range independent background subtraction algorithm (RIA) [15] in order to eliminate the fluorescence background. The underlying basis of RIA is iterative smoothing of the measured raw Raman spectrum. The RIA method uses a model based on modified iterative smoothing of the measured Raman spectrum in such a manner that the high-frequency Raman peaks are gradually eliminated finally leaving the underlying broad baseline which can be subtracted from the raw spectrum to yield the true Raman signal. Each background-subtracted sample Raman spectrum was subjected to standard normal variate (SNV) transformation [16] to reduce baseline offset effects.

2.5. Data Analysis

The use of depth-sensitive Raman spectra for discrimination of cancerous and normal FFPE tissue blocks requires a diagnostic algorithm which seeks to extract the diagnostic features from the measured set of spectra and classify them into appropriate pathologic categories. A probability based multivariate diagnostic algorithm was developed for analyzing the diagnostic content of the depth-sensitive Raman spectra measured from the different FFPE tissue blocks. The algorithm development consisted of two steps: i) feature extraction (or dimensionality reduction) through principal component analysis (PCA) and ii) probabilistic classification via sparse multinomial logistic regression (SMLR). These techniques have been described in detail elsewhere [17-19]. In brief, PCA [17] is a linear feature extraction procedure that aims to find a set of linear transformations on the input data that contains the maximum information about the data in a reduced dimensionality space. SMLR [18] is a Bayesian machine learning framework that separates a set of input data into its constituent classes by computing the posterior probabilities of their class membership based on a labelled training set data.

Principal Component Analysis (PCA)

In the case of Raman spectral data X with dimension N = 1000, the objective of PCA is to find a transformation $\mathbf{\Phi_M}$ such the new M-dimensional (M<N) random vector $\mathbf{Y_M} = \mathbf{\Phi_M}^T\mathbf{X}$ contains the maximum information about **X**. To find Φ_M the mean square error between **X** and the approximation $\mathbf{X}^{/} = \mathbf{\Phi_M Y_M}$ is minimized. In other words, $\mathbf{\Phi_M}$ is selected such that $E[(\mathbf{X}-\mathbf{X}^{/})^2] = E[(\mathbf{X}-\mathbf{\Phi_M Y_M})^2]$ is the minimum. This solution for $\mathbf{\Phi_M}$ is obtained from the eigenvalue-eigenvector equation $\mathbf{C\Phi_M} = \mathbf{\Lambda\Phi_M}$, where $\mathbf{\Lambda}$ was a diagonal matrix whose elements are the eigenvalues of the covariance matrix $\mathbf{C} = E[\mathbf{XX}^T]-\boldsymbol{\mu\mu}^T$, $\boldsymbol{\mu}$ being the mean of the input spectral data matrix. The columns of $\mathbf{\Phi_M}$ solution are the M eigenvectors of **C** with largest eigen values and are called the principal components (PC). This solution also maximizes the variance of the output random vector or the principal component scores in the $\mathbf{Y_M} = \mathbf{\Phi_M}^T\mathbf{X}$ transformed space, i.e. it maximizes $E[\mathbf{YY}^T]$.

Sparse Multinomial Logistic Regression (SMLR)

The central idea of sparse multinomial logistic regression **(**SMLR) is to separate a set of labelled input data into its constituent classes by predicting the posterior probabilities of their class-membership. It computes the posterior probabilities using a multinomial logistic regression model and constructs a decision boundary that separates the data into its constituent classes based on the computed posterior probabilities following Bayes' rule. Classification of a given set of input data **x** is based on the vector of posterior probability estimates yielded by the SMLR algorithm and a class is assigned to each dataset (transformation of the original spectrum) for which its posterior probability is the highest.

All the discrimination analyses were performed using leave-one-block-out cross validation. The predictive accuracies of the diagnostic algorithm used for different classification tasks were calculated with respect to histopathology report as the reference gold standard.

3. RESULTS

The Raman spectra were measured from the different depths of the FFPE tissue blocks by axially varying the focal spot of the illumination beam in steps of 10 µm for 0-200 µm depth, 20 µm for 200-300 µm depth and 50 µm for higher depths of up to ~500 µm. Figure **2a** shows the typical depth-sensitive Raman spectra measured from a cancerous FFPE tissue block chosen at random from among the seven different blocks belonging to the same pathology. Similarly, Figure **2b** shows the typical Raman spectra measured from a normal FFPE tissue block randomly selected from among the remaining seven blocks of normal breast tissues. The spectra in each of the tissue blocks were measured at two different lateral positions separated by ~0.5 mm from each other.

Figure **3a** shows the conventional Raman spectrum of native paraffin (comprising the tissue blocks) measured with the same experimental set-up. The

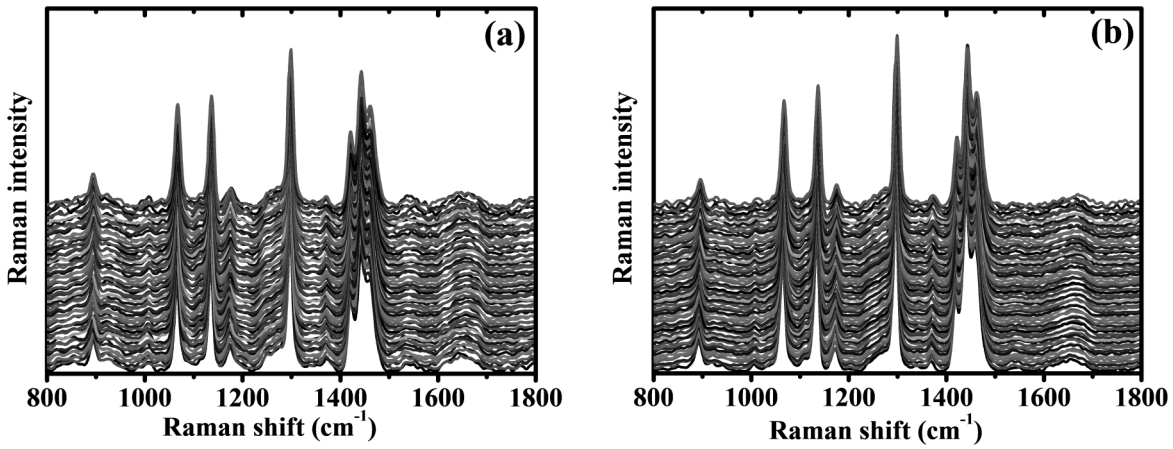

Figure 2: (**a**) Raman spectra corresponding to different depths of a cancerous FFPE tissue block measured at two different lateral sites. The spectra are shown with offset for clarity. (**b**) Raman spectra corresponding to different depths of a normal FFPE tissue block measured at two different lateral sites. The spectra are shown with offset for clarity.

spectrum is the average of the spectra measured from the non-tissue containing portion of a total of 14 FFPE blocks. From each block three spectra were recorded from three different lateral positions containing only paraffin but no tissue. It is evident from the Figures **2a** and **2b** that the Raman spectra of the FFPE tissue blocks at all the depths irrespective of the tissue type are dominated by the Raman signatures characteristic of paraffin except at ~1650 cm^{-1} where the tissue Raman band believed to be due to proteins (amide-I) [3-4, 20] is distinctly present. However, the band does not seem to reveal any inter-category differences apparently being masked by the presence of the strong paraffin Raman bands. Figure **3b** shows the mean Raman spectra of cancerous and normal breast tissue types obtained by averaging the respective set of spectra of each of the Figures **2a** and **2b** corresponding to cancerous and normal FFPE tissue block. Although not in a great way but it is certainly apparent from the figure that the intensity of the 1650 cm^{-1} band is enhanced, consistent with that reported in literature [3, 20], in the cancerous as compared to that in the normal FFPE tissue block. Similarly, the intensity of the Raman peak ~1265 cm^{-1}, believed to be due to amide-III [3-4, 20], is also seen to be more in cancerous relative to the normal breast tissue block.

As the depth at which the tissue was embedded in a FFPE tissue block was not known and visibly seen to vary across the blocks investigated, it was imperative to locate by some means the axial position of the tissue in each FFPE block. In order for that we devised a scheme which sought to find out, in each tissue block, the subset of spectra (from among the whole set of

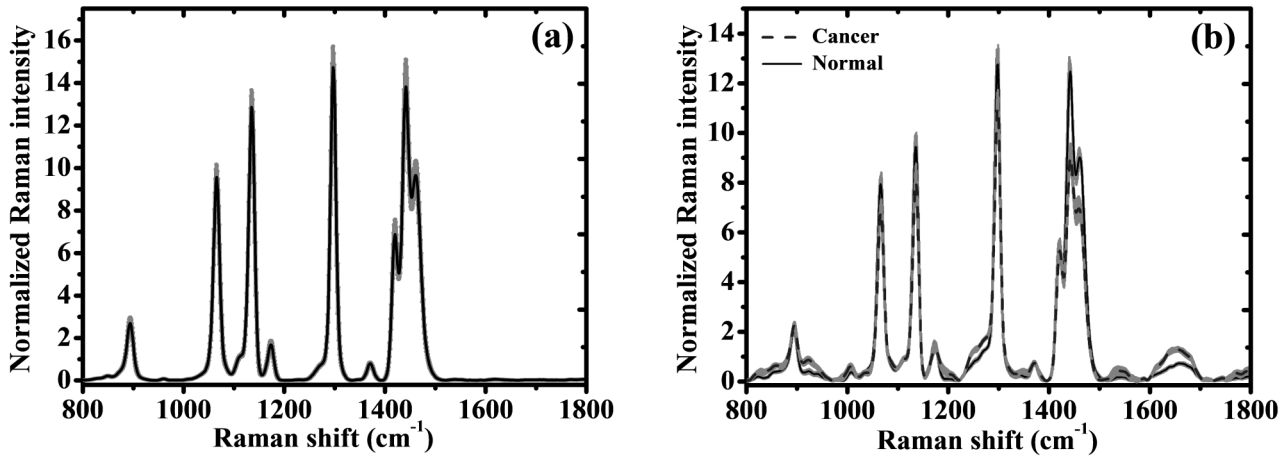

Figure 3: (**a**) Normalized Raman spectrum of paraffin (comprising the tissue blocks). The spectrum is the average of the spectra measured from the non-tissue containing portion of a total of fourteen FFPE blocks with each block containing three lateral measurement sites. The error bars shown in grey represent ±1 standard deviation. (**b**) Mean Raman spectra of cancerous (dashed line) and normal (solid line) FFPE tissue blocks obtained by averaging the respective set of spectra shown in Figures **2a** and **2b**. The error bars shown in grey represent ±1 standard deviation. The spectra are mean-normalized.

measured depth-sensitive Raman spectra) that contained the most of the tissue specific Raman signatures. Since the Raman bands around 1650 cm^{-1} and 1135 cm^{-1} are known primarily to be characteristics of tissue and paraffin respectively, the ratio of the peak intensities at these two wavenumbers (i.e. I_{1650}/I_{1135}), indicative of the content of tissue Raman signatures in the spectra, was plotted against the axial positions for the whole set of depth-sensitive spectra measured in each block. Figure **4a** shows the plot of the ratio verses the axial position for the set of spectra of three cancerous and three normal tissue blocks chosen at random from among the fourteen tissue blocks. One may see that irrespective of the blocks investigated, the ratio values first increase, reach a maximum and then decrease implying that the spectra corresponding to the ratio values around the maximum best contain the tissue specific signatures. Further one can also see that the maximum occurs at different axial positions for the different FFPE tissue blocks signifying the variation in the subsurface positions of tissue in the different blocks. In order to find out the set of spectra that is most representative of tissue, only those spectra in each block were retained for which the ratio values were more than or equal to 90% of their respective maxima. Figure **4b** shows the shortlisted spectra (most representative of tissue) corresponding to the tissue blocks whose depth-sensitive Raman spectra are shown in Figures **2a** and **2b**.

In order to de-paraffinize the measured Raman spectra, the full set of depth-sensitive Raman spectra of the FFPE tissue blocks was subjected to the method of scale-subtraction [13]. In this technique, the mean Raman spectrum of paraffin, obtained for an FFPE tissue block, was subtracted from each of the measured depth-sensitive Raman spectra of that particular tissue block after scaling the peak intensity of the 1135 cm^{-1} Raman band (unique to paraffin) of this spectrum to the same height as that of the paraffin Raman spectrum. For a given tissue block spectrum, the peak intensity was scaled to the same height as that of the paraffin spectrum by first estimating the ratios of the peak to the integrated intensity of this spectrum as well as of the mean paraffin Raman spectrum over the spectral region of 800-1800 cm^{-1} and then multiplying the intensities of the tissue block spectrum with the ratio estimated from the paraffin spectrum and the corresponding Raman intensities of the paraffin spectrum with the ratio value obtained from the tissue block spectrum. Figure **5a** shows the Raman spectra retrieved through scale-subtraction from the spectra shown in Figure **4b**. It is apparent from the figures that the retrieved spectra resemble the typical Raman spectra of breast tissues reported in literature [20] except for the few sharp spikes with intensities extending even in the negative. These spikes are the unavoidable artefacts that result during scale-subtraction from those parts of the characteristic paraffin Raman bands which slightly differ in line shape than that of the corresponding paraffin Raman bands contained in the Raman spectra of the FFPE tissue blocks and as a result do not have complete overlap with their contours. Though appropriate spectral smoothening can reduce the height of these spikes or even eliminate them in some situations but the process almost flattens many of the tissue specific spectral signatures resulting in further distortions in the

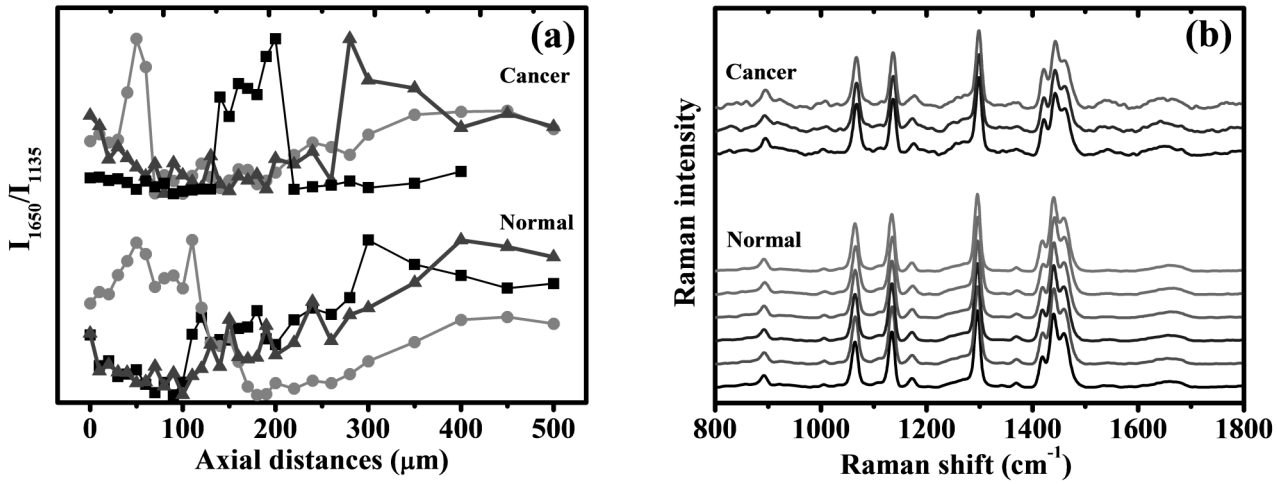

Figure 4: (**a**) Plot of the ratio (I_{1650}/I_{1135}) versus the axial position for the set of spectra of three cancerous (upper panel) and three normal (lower panel) tissue blocks chosen at random from among the fourteen tissue blocks. (**b**) Shortlisted spectra (most representative of tissue) corresponding to the Raman spectra shown in Figures **2a** and **2b**. The spectra are shown with an offset for clarity.

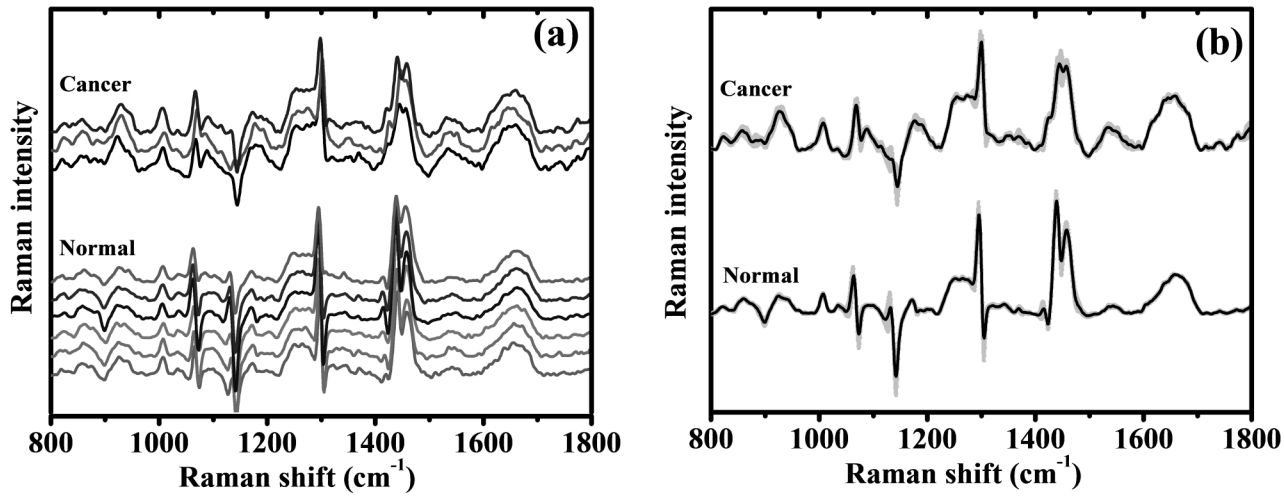

Figure 5: (**a**) Raman spectra of cancer (upper panel) and normal (lower panel) breast tissues retrieved through scale-subtraction from the shortlisted spectra shown in Figure **4b**. The spectra are shown with an offset for clarity. (**b**) Mean scale-subtracted Raman spectra of cancerous (upper panel) and normal (lower panel) breast tissues obtained by averaging the respective set of spectra of the tissue types shown in Figure **5a**. The error bars shown in grey represent ±1 standard deviation.

scale-subtracted spectra. Figure **5b** shows the average scale-subtracted spectra corresponding to those shown in Figure **5a**. One may note that significant spectral differences which otherwise were completely masked before scale-subtraction are now explicit in all the Raman bands of the tissue types. For example, significant spectral variations are seen around 1100 to 1300, 1440 and 1650 cm^{-1} and they correspond to biochemical differences inherent in the different breast tissues, notably connective tissue proteins, and fatty acids [3, 20]. The ratios of peak intensities at 1650 cm^{-1} and 1450 cm^{-1} (i.e. I_{1650}/I_{1450}), estimated from the whole set of scale-subtracted spectra of the tissue types and reflecting the relationship between relative protein and lipid content, were found to be significantly ($p<0.05$) different in normal as compared to the cancerous tissue spectra. It is pertinent to mention here that this observation is in line with that reported in literature [3, 20] where it has also been proposed as an index for discriminating cancerous from normal breast tissues. For assessing the ability of I_{1650}/I_{1450} for possible discrimination between tissue types in the present case, its values were used as input to a nearest-mean classifier (NMC). Table **1** shows the discrimination results obtained with the values of I_{1650}/I_{1450} as input to a nearest-mean classifier employed in a leave-one-block-out cross validation mode. It is seen that the values of sensitivity and specificity towards cancer are ~77% and 56% respectively.

In order to evaluate the diagnostic content of the whole range of normalized intensities contained in the Raman spectra measured from the FFPE tissue blocks, the full set of shortlisted (most representative of tissue) scale-subtracted spectra of the tissue blocks was subjected to the input of the PCA-SMLR based probabilistic multivariate diagnostic algorithm developed for this purpose. The task of the algorithm was to classify the tissue spectra into two pathologic categories: cancerous and normal. PCA of the set of shortlisted scaled-subtracted spectra resulted in forty principal components that collectively accounted for 99.9% of the total variance of the spectral data. Of these forty principal components, only six (having largest eigen-values and accounting for ~90% of the total variance) were retained since they were found to yield optimum classification between the tissue types using the SMLR based classification. Table **2** shows the classification results listing sensitivity, specificity, positive predictive value (PPV), negative predictive value (NPV) and overall accuracy. The classification results were obtained based on leave-one-block-out

Table 1: The discrimination results obtained using the nearest mean classifier (NMC) with the values of the ratio I_{1650}/I_{1450} as its input. The results are based on leave-one-block-out cross validation

Classification algorithm	Sensitivity (N=22)	Specificity (N=18)	Positive predictive value (N=25)	Negative predictive value (N=15)	Overall accuracy (N=40)
Ratio (I_{1650}/I_{1450}) - NMC	77%	56%	68%	67%	68%

Table 2: The discrimination results obtained (i) using PCA-SMLR applied on the shortlisted set of scale-subtracted, depth-sensitive Raman spectra of the FFPE tissue blocks of pathologically certified cancerous and normal breast tissues and (ii) using SMLR with the ratioI_{1650}/I_{1450} as its input. The results are based on leave-one-block-out cross validation

Classification algorithm	Sensitivity (N=22)	Specificity (N=18)	Positive predictive value	Negative predictive value	Overall accuracy (N=40)
PCA-SMLR	96%	100%	100%	95%	98%
Ratio (I_{1650}/I_{1450}) - SMLR	59%	72%	72%	59%	65%

cross validation of the PCA-SMLR algorithm on the entire data set. The results show an excellent ability for the depth-sensitive Raman spectra to evaluate pathology status in FFPE tissue blocks, with 96% sensitivity and 100% specificity, and an overall classification accuracy of 98%. Alternatively, the discrimination was performed with 95% NPV and 100% PPV. For the sake of comparison, the discriminations results obtained using the values of I_{1650}/I_{1450} as input to the SMLR classifier are also listed in Table **2**. One can see that the sensitivity and specificity values (59% and 72% respectively) yielded by the single-variate algorithm are significantly poorer as compared to the PCA-SMLR based multivariate algorithm.

In addition to assigning class labels, the PCA-SMLR based diagnostic algorithm also yielded posterior probabilities of the measured tissue sites belonging to each class of breast tissues. Figure **6** illustrates the posterior probabilities computed by the algorithm for the measured tissue spectra of each tissue class of belonging to cancer. While the open symbols in the figures represent probabilities of correct class-membership, the closed symbols denote the probabilities for the misclassified tissue sites. The figure indicates that 96% of the cancerous breast tissue sites have a posterior probability >0.5 and 100% of the normal breast tissue sites have a posterior probability <0.5. A further examination of the figure reveals an interesting observation. While all the normal tissue sites are seen to have a posterior probability <0.2 of being cancer, only 20 out of 22 of the cancerous sites are found having a posterior probability >0.8. Of the remaining two cancerous sites, while one is seen to have a probability of ~0.65 of being cancer, the corresponding probability for the other is seen to be exceedingly low (<0.1). This is not quite unusual because while the presence of any amount cancerous cells is not expected in a normal breast tissue, the reverse is not guaranteed. A piece of cancerous tissue due to its very heterogeneous nature might contain variable amount of normal cells at some isolated locations across the investigational volume which otherwise is cancerous. A further proof towards this is the fact that the sensitivity was seen to rise to 100% (with the posterior probability >0.8 for all) when the discrimination analysis was carried out on the basis of "averaged-spectrum-per-block" by applying the algorithm on the spectral data obtained by averaging over the shortlisted set of spectra in each of the cancerous and normal tissue blocks thereby generating a single spectrum per block.

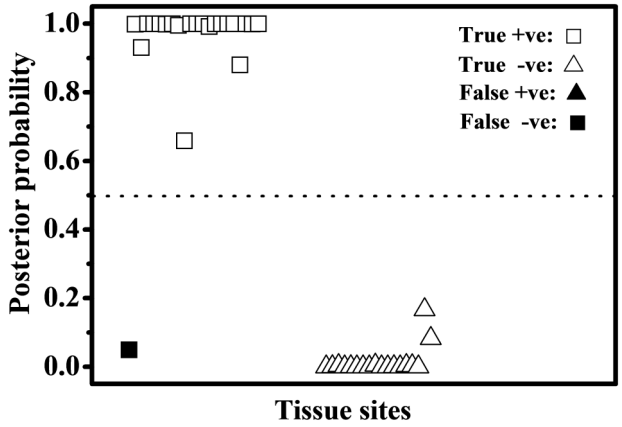

Figure 6: Posterior probabilities of belonging to cancer as computed by the PCA-SMLR algorithm for the scaled-subtracted spectra of each tissue category. The open symbols represent probabilities of correct class-membership (true positives and true negatives) and the closed symbols denote the probabilities for misclassification (false positives and false negatives).

4. DISCUSSIONS

At present there exists no method for determining the pathologic state of a paraffin embedded tissue without preparing micro-thin slices from an intact FFPE tissue block and subjecting it to further processing. The present study is a step towards investigating the feasibility of such a task using the technique of Raman spectroscopy. The goal of the present study is to explore the capability of Raman spectroscopy for discriminating the cancerous from normal human breast tissues based on depth-sensitive measurement of Raman spectra from the intact FFPE tissue blocks. Such an approach is all the more desired because it is

completely non-destructive as it eliminates the need to prepare micro-thin tissue slices thereby enabling preservation of the tissue blocks intact for further use in future in case any re-assessment is required.

The depth-sensitive Raman spectra measured from the FFPE blocks of pathologically certified cancerous and normal breast tissues were found to be severely contaminated (see Figures **2a** and **2b**) by the Raman signatures of paraffin whose Raman cross-section is known to be significantly higher than that of the biological tissues. In order to eliminate the paraffin Raman background and isolate the weak tissue Raman signatures buried in it, the Raman spectrum of paraffin measured from the non-tissue containing region of the block was scaled-subtracted from the measured depth-sensitive Raman spectra of the FFPE tissue blocks. The method was found to satisfactorily recover the Raman spectra characteristic of breast tissues by cancelling out the spectral contributions of paraffin contained in it. It is important to mention here that mathematical de-praffinization was earlier attempted by the Michel Manfait group [9-11]. They employed ICA to first generate model sources of paraffin from the set of measured micro-Raman spectra of the micro-thin tissue sections and then used these model paraffin spectra along with the set of micro-Raman spectra, from which they were derived, as input to a non-negatively constrained least-squares method [9-11] for obtaining de-praffinized Raman spectra of tissues. However, the major disadvantage of this approach is that ICA being based on the theory of statistical pattern recognition requires an array of Raman spectra at its input for generating the model source spectra of paraffin. Further, the scale of accuracy of the source spectra is dependent on the size of the input Raman spectral data which needs to be larger than the data dimension (i.e. number of wavenumbers) to satisfy the validity criteria of ICA. In contrast, the present method of mathematical de-praffinization employed by us is non-statistical and requires only two spectra, a paraffin Raman spectrum which can be easily obtained from the non-tissue containing part of the FFPE tissue block and a depth-sensitive Raman spectrum measured across the tissue containing portion of the block.

It is also important to mention here that instead of using the mean paraffin Raman spectrum obtained by averaging all the paraffin Raman spectra of the different FFPE blocks investigated, the mean paraffin Raman spectrum of an individual FFPE block was used for generating the scaled-subtracted spectra from the measured set of depth-sensitive spectra from that block. This is to minimize the effect of the observed inter-block variability (~9-20%) of the line-shapes of the paraffin Raman bands on the outcome of scaled-subtraction. However, the scaled-subtracted spectra still showed a few sharp spikes with intensities extending even in the negative (Figure **5a**). These are unavoidable because during scaled-subtraction even a very subtle mismatch between the line shape of the characteristic paraffin Raman bands appearing in the spectra measured from non-tissue and tissue containing part of the FFPE block is bound to lead to this kind of artefacts. Though a direct comparison is not possible, it is pertinent to mention here that the de-paraffinized spectra obtained by the Michel Manfait group [9-11] using non-negatively constrained least square method also had similar sharp spikes across the spectral range. However, these artefacts were observed to have no bearing on the results of discrimination.

In order to discriminate the FFPE tissue blocks two different approaches were taken. Under the first approach, there were two sub-approaches. The first sub-approach was empirical wherein a geometric classifier (nearest mean classifier) was used and the values of the ratio of intensities at 1650 cm^{-1} and 1450 cm^{-1} (i.e. I_{1650}/I_{1450}) computed from the measured set of spectra were used as input to the classifier. The second sub-approach was a mix of empirical and statistical wherein an SMLR based classifier was applied on the same set of ratio values as its input. In the second approach, which was purely statistical, the normalized Raman intensities over all the wavenumbers were used as an input to a multivariate statistical diagnostic algorithm developed based on PCA and SMLR. The objective of the first approach was to evaluate the discrimination efficacy of the intensity ratio that was observed to be significantly different for the cancerous FFPE tissue block than the normal. The advantage of using such a diagnostic feature based only on the intensity ratio is that it could considerably simplify the experimental arrangement since no spectral resolution is required. The second approach exploits the total spectral information content of the full range of spectral data. The results (Table **2**) clearly indicate that multivariate algorithms based on PCA-SMLR provides significantly improved discrimination accuracy. This is quite expected because in contrast to the case where the classifier (either geometric or statistical) uses only a single spectral variable (e.g. the ratio of intensity), PCA-SMLR uses multiple Raman bands over the full range of

wave-numbers thereby exploiting significantly more information useful for discrimination.

Classification error is the ultimate measure of performance of a diagnostic algorithm and it strongly depends on the mathematical formulation of the algorithm. In practice, the classification error is estimated from all the available data that include both the training and validation sets [19]. An algorithm is considered robust when it can provide a reliable estimate of classification error independent of the sizes of both the training as well as the validation set data. This depends on the ability of the algorithm to eliminate the high degree of multi-collinearity that is usually present in the measured spectral data whose dimension is higher compared to its size (i.e. the number of measurements). The major advantage of using the SMLR based classification is that it can mitigate this collinearity problem [18-19] and therefore, can perform classification from a set of test data of any size and dimension with sufficient accuracy. The additional advantage of the algorithm is that it also predicts the posterior probability of tissues belonging to a specific diagnostic category thus allowing one to quantitatively assess the certainty of classification [18-19]. This is apparent from Figure **6** where the posterior probabilities (of being cancer) as predicted by the PCA-SMLR algorithm are plotted for the scaled-subtracted, depth-sensitive spectra of FFPE tissue blocks. Knowledge of the posterior probability of class-membership is useful in a clinical pathological setting because it would allow to reassess those sites that are classified with higher relative uncertainty, provide the opportunity to improve performance by rejecting more ambiguous data points, cause an optimal compensation for asymmetric misclassification costs and varying class proportions and allow for the fusion of outputs with other probabilistic sources of information before applying the decision criteria.

An important task while using a diagnostic algorithm is to evaluate the generalized classification ability of the algorithm. It was thus required to make sure that the validation set data was fully independent of the training set data i.e. it should not contain any of the pieces of the training set data with which the algorithm was trained and optimized. The independence was ensured by following the leave-one-block-out cross validation method. In this method, for each of the N (= 14) blocks of Raman spectra, spectra of N-1 (= 13) of them were used to train the algorithm and the set of spectra of the remaining block was left excluded (and therefore not used by the algorithm during calibration) as the validation set. This was repeated N times (until the spectra of all the withheld blocks were predicted) each time excluding a different block for the purpose of validation and retraining the algorithm using spectra of the rest of the blocks. Since the training set data remained completely independent of the test data in each of the N loops (as the set of spectra from a block was never a part of both the training and the validation sets simultaneously), the validation was statistically unbiased. Thus, classification results obtained in the present study can be considered reliable in predicting future classification performance.

The results of our studies show that the depth-sensitive Raman technique combined with the PCA-SMLR algorithm can discriminate cancerous from normal breast tissue blocks with an accuracy of >98% with the shortlisted set of scaled-subtracted spectra of the FFPE tissue blocks, while a sensitivity and specificity towards cancer of 100% was obtained when the algorithm was applied on the set of spectra obtained by averaging over the shortlisted spectral set in each of the cancerous and normal tissue blocks thereby generating a single spectrum per block. However, it should be noted that the diagnostic algorithm used in this study was based on depth-sensitive Raman spectra from a limited number of FFPE tissue blocks assumed to be representative of the entire population. The selection of the FFPE tissue blocks as well as the limited number of spectra in each block might influence the discrimination results obtained in this study. Further, the intrinsic variability of the Raman spectra that might result due to variations in the FFPE tissue blocks also might affect the results of our study. Therefore, further studies in a larger sample size, which are already in progress, will be used to address these issues and validate the classification results presented here.

5. CONCLUSIONS

A preliminary study was carried out for evaluating the applicability of Raman spectroscopy to discriminate cancerous and normal breast tissues using depth-sensitive Raman spectra measured from the FFPE tissue blocks. The important attraction of the approach is that it enables tissue analysis using intact tissue blocks without requiring preparation of any thin tissue sections or any other processing, and is also capable of providing a quantitative diagnostic feedback. Use of a diagnostic algorithm developed using the framework of PCA and SMLR provided a sensitivity of 96% and a specificity of 100% towards cancer based on leave-

one-block-out cross validation. When the discrimination analysis was carried out on the basis of a single spectrum per block, a sensitivity and specificity towards cancer of 100% was obtained. The Bayesian framework of SMLR formulation made it possible to predict the posterior probability of class membership in discriminating cancerous from the normal breast tissue sites. Overall, the results of the present work indicate that the combination of depth-sensitive Raman spectroscopy and a multivariate statistical diagnostic algorithm could be a promising tool in a clinical pathology setting for non-destructively determining the pathologic state of a tissue embedded in intact FFPE blocks.

ACKNOWLEDGEMENTS

The authors would like to thank Mr. Surjendu B. Dutta for his help at various stages of the experiment. They would also like to thank the staff of the Department of Pathology, Mahatma Gandhi Memorial Medical College for their active cooperation and help.

REFERENCES

[1] Bancroft JD, Gamble M. Theory and Practice of Histological Techniques. 6th ed. Philadelphia: Elsevier's Health Sciences 2008.

[2] Kiernan JA. Histological and Histochemical Methods: Theory and Practice. 5th ed. Banbury: Scion 2015.

[3] Manoharan R, Wang Y, Feld MS. Histochemical analysis of biological tissues using Raman spectroscopy. Spectrochim Acta Part A 1996; 52: 215-49. http://dx.doi.org/10.1016/0584-8539(95)01573-6

[4] Faolain EO, Hunter MB, Byrne JM, *et al.* Raman spectroscopic evaluation of efficacy of current paraffin wax section dewaxing agents. J Histochem Cytochem 2005; 53: 121-9. http://dx.doi.org/10.1369/jhc.4A6536.2005

[5] Krishna CM, Sockalingum GD, Venteo L, *et al.* Evaluation of the suitability of ex vivo handled ovarian tissues for optical diagnosis by Raman microspectroscopy. Biopoly 2005; 79: 269-76. http://dx.doi.org/10.1002/bip.20346

[6] Tan KM, Herrington CS, Brown CTA. Discrimination of normal from pre-malignant cervical tissue by Raman mapping of de-paraffinized histological tissue sections. J Biophot 2011; 4: 40-8. http://dx.doi.org/10.1002/jbio.201000083

[7] Rashid N, Nawaz H, Poon KWC, *et al.* Raman microspectroscopy for the early detection of pre-malignant changes in cervical tissue. Exp Mol Pathol 2014; 97: 554-64. http://dx.doi.org/10.1016/j.yexmp.2014.10.013

[8] Lyng F, Traynor MD, Ramos IRM, Bonnier F, Byrne HJ. Raman spectroscopy for screening and diagnosis of cervical cancer. Anal Bioanal Chem 2015; 407: 8279-89. http://dx.doi.org/10.1007/s00216-015-8946-1

[9] Vrabie V, Gobinet C, Piot O, *et al.* Independent component analysis of Raman spectra: application on paraffin-embedded skin biopsies. Biomed Signal Process Control 2007; 2: 40-50. http://dx.doi.org/10.1016/j.bspc.2007.03.001

[10] Tfayli A, Gobinet C, Vrabie V, Huez R, Manfait M, Piot O. Digital dewaxing of Raman signals: discrimination between nevi and melanoma spectra obtained from paraffin-embedded skin biopsies. Appl Spectrosc 2009; 63: 564-70. http://dx.doi.org/10.1366/000370209788347048

[11] Gobinet C, Vrabie V, Manfait M, Piot O. Preprocessing methods of Raman spectra for source extraction on biomedical samples: application on paraffin-embedded skin biopsies. IEEE Trans Biomed Eng 2009; 56: 1371-82. http://dx.doi.org/10.1109/TBME.2009.2014073

[12] Khan KM, Krishna H, Majumder SK, Rao KD, Gupta PK. Depth-sensitive Raman spectroscopy combined with optical coherence tomography for layered tissue analysis. J Biophot 2014; 7: 77-85. http://dx.doi.org/10.1002/jbio.201200208

[13] Khan KM, Majumder SK, Gupta PK. Cone–shell Raman spectroscopy (CSRS) for depth-sensitive measurements in layered tissue. J Biophot 2015; 8: 889-96. http://dx.doi.org/10.1002/jbio.201400125

[14] Fryling M, Frank CJ, McCreeey RL. Intensity calibration and sensitivity comparisons for CCD/Raman spectrometers. Appl Spectrosc 1993; 47: 1965-74. http://dx.doi.org/10.1366/0003702934066226

[15] Krishna H, Majumder SK, Gupta PK. Range-independent background subtraction algorithm for recovery of Raman spectra of biological tissue. J Raman Spectrosc 2012; 43: 1884-94. http://dx.doi.org/10.1002/jrs.4127

[16] Barnes RJ, Dhanoa MS, Lister SJ. Standard normal variate transformation and de-trending of near-infrared diffuse reflectance spectra. Appl Spectrosc 1989; 43: 772-7. http://dx.doi.org/10.1366/0003702894202201

[17] Jolliffe IT. Principal Component Analysis. 2nd ed. New York: Springer 2002.

[18] Krishnapuram B, Cari L, Figueiredo MAT. Sparse multinomial logistic regression: Fast algorithums and generalization bounds. IEEE Trans Pattern Anal Machine Intell 2005; 27: 957-68. http://dx.doi.org/10.1109/TPAMI.2005.127

[19] Majumder SK, Gebhart SC, Johnson MD, Thompson R, Lin WC, Mahadevan-Jansen A. A probability-based spectroscopic diagnostic algorithm for simultaneous discrimination of brain tumor and tumor margins of normal brain tissue. Appl Spectrosc 2007; 61: 548-57. http://dx.doi.org/10.1366/000370207780807704

[20] Peltier KES, Haka AS, Fitzmaurice M, *et al.* Raman microspectroscopic model of human breast tissue: implications for breast cancer diagnosis *in vivo*. J Raman Spectrosc 2002; 33: 552-63. http://dx.doi.org/10.1002/jrs.877

Received on 20-05-2016 Accepted on 20-07-2016 Published on 18-11-2016

http://dx.doi.org/10.6000/1927-7229.2016.05.04.4